Biophysical Journal Volume 105 July 2013 494–501

Disruption of Intrinsic Motions as a Mechanism for Enzyme Inhibition

Rebecca J. Swett, G. Andrés Cisneros, and Andrew L. Feig*
Department of Chemistry, Wayne State University, Detroit, Michigan

ABSTRACT *Clostridium difficile (C. diff)* is one of the most common and most severe hospital-acquired infections; its consequences range from lengthened hospital stay to outright lethality. *C. diff* causes cellular damage through the action of two large toxins TcdA and TcdB. Recently, there has been increased effort toward developing antitoxin therapies, rather than antibacterial treatments, in hopes of mitigating the acquisition of drug resistance. To date, no analysis of the recognition mechanism of TcdA or TcdB has been attempted. Here, we use small molecule flexible docking followed by unbiased molecular dynamics to obtain a more detailed perspective on how inhibitory peptides, exemplified by two species HQSPWHH and EGWHAHT function. Using principal component analysis and generalized masked Delaunay analysis, an examination of the conformational space of TcdB in its apo form as well as forms bound to the peptides and UDP-Glucose was performed. Although both species inhibit by binding in the active site, they do so in two very different ways. The simulations show that the conformational space occupied by TcdB bound to the two peptides are quite different and provide valuable insight for the future design of toxin inhibitors and other enzymes that interact with their substrates through conformational capture mechanisms and thus work by the disruption of the protein's intrinsic motions.

INTRODUCTION

Clostridium difficile (*C. diff*) is recognized as a widespread problem due to its ability to cause hospital-acquired infections (1–4). An opportunistic pathogen, *C. diff* primarily affects patients taking, or having recently completed, a course of broad-spectrum antibiotics (4). The extensive tissue damage caused by the *C. difficile* toxins produced results in the collection of diseases collectively recognized as CDAD, or *Clostridium difficile*-associated diseases. Development of antivirulence therapies as opposed to antibiotics may be an effective way of mitigating the damage of an infection without inciting further antibiotic resistance (5,6). Toxins A and B (TcdA and TcdB) are responsible for the bulk of the cellular damage that occurs upon infection, and thus are excellent targets for development of antitoxin therapies.

The overall structure of TcdB is shown in Fig. 1. The four domains are shown in panel *A* and include a C-terminal repetitive oligopeptide (CROP) domain, a translocation domain, a cysteine protease domain, and a glucosyltransferase domain. Both TcdA and TcdB follow this global organization, and have a conserved sequence similarity of roughly 73% in their catalytic domain (7). For the purposes of antitoxin therapies, our primary target is the glucosyltransferase domain; however, work on the other domains is forthcoming. Structural elements within the glucosyltransferase domain relevant to our analyses are presented in panel *B*. The mobile loop (*yellow*), supports the catalytically relevant DXD motif, and has been described in detail previously (8). Two regions involved in RhoA binding/substrate recognition are shown in green and red. The N-terminal four-helix bundle shown in blue has been implicated in membrane association (9). The two upper regions shown in cyan constitute features that do not appear in homologous glucosyltransferases, and thus are unique to the *C. diff* toxins but have no known function currently. The β-hairpin shown in purple is known as the active site flap, and may be involved in excluding improper substrates and order of binding. Panel *C* shows the orientation of the substrate UDP-Glucose (UPG), with respect to the mobile loop and active site flap based on recent cocrystal structures (10).

Delivery of the glucosyltransferase domain to the cytosol is of interest with respect to drug design as it has implications for the folding and flexibility of the catalytic subunit. This process has been studied in significant detail (7,8,10–12). One of the critical steps involves passing the catalytic glucosyltransferase domain through a membrane pore composed of the translocation domain, allowing the toxin to escape from the endosome. In light of the pore translocation that occurs, it is to be expected that the glucosyltransferase must have either a very flexible structure, or a fold that can be significantly altered by pH. This is of particular interest when paired with the nature of the enzymes that it targets. Small G-proteins are highly flexible and have been shown to use a conformational selection mechanism rather than a typical induced fit or lock and key mechanism (13). It is a fair hypothesis that TcdB might also employ a conformational selection mechanism to match the types of motions exhibited by its target.

We recently characterized the large-scale molecular motions that occur in the glucosyltransferase domain of TcdB, alone and in contact with RhoA using long-timescale molecular dynamics (MD) simulations (14).The effect of large-scale conformational changes on the active site and RhoA binding were determined, but the effects of

Submitted January 18, 2013, and accepted for publication May 20, 2013.
*Correspondence: afeig@chem.wayne.edu
Editor: Gerhard Hummer.

0006-3495/13/07/0494/8 $2.00
http://dx.doi.org/10.1016/j.bpj.2013.05.031

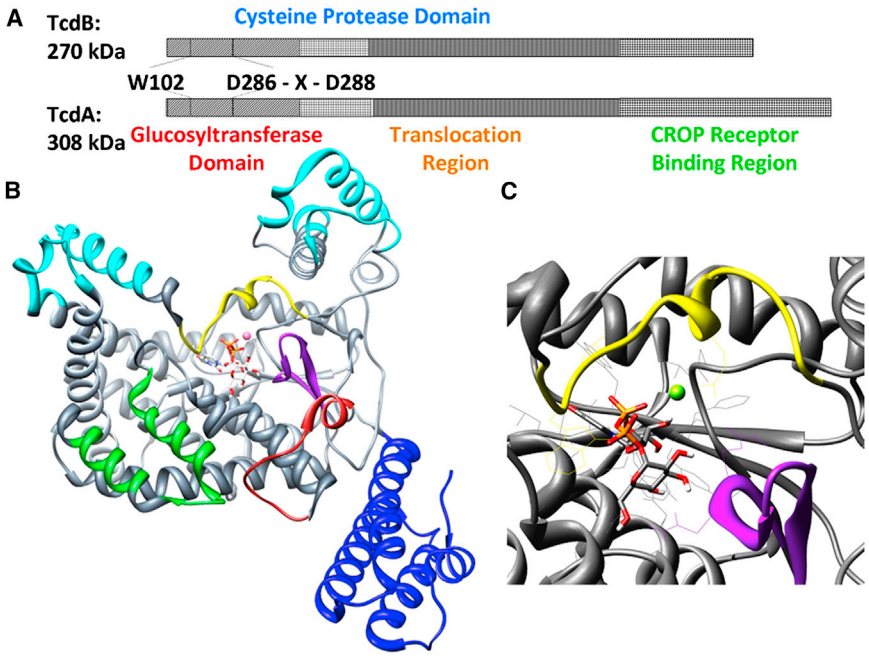

FIGURE 1 Domain organization of *C. difficile* toxins, structure of *C. difficile* Toxin B glucosyltransferase domain (TcdB) PDBID: 2BVL. Panel *A*:Toxins A and B share a common domain organization, differing in the size of the CROP receptor binding region. The glucosyltransferase domain is cleaved from the translocation and CROP domains by the cysteine protease domain upon endocytosis. Panel *B*: Structure of the glucosyltransferase domain. Toxin-specific upper promontories shown in cyan, DXD supporting mobile loop shown in yellow, active site flap shown in purple, protein-protein recognition loops shown in green and red, and N-terminal four helix bundle shown in blue. Panel *C*. Inset showing orientation of UDP-glucose in the active site, relative to the mobile loop and active site flap.

UDP-glucose were not assessed in that study. As a conformational selection mechanism is suspected, the effects of substrate binding on large-scale conformational motions are of great interest.

A protein that employs a conformational selection mechanism occupies a large conformational space, which is then restricted or modified by interactions with its substrates or binding partners (15). To understand known substrates and develop novel binding partners such as inhibitors, it is necessary to recognize the malleability of the active site and thoroughly understand the consequences of each internal motion and interaction. One avenue to evaluate the available conformational space and understand how it is affected by substrate binding involves using a combination of MD, General Masked Delaunay (GMD) analysis, and principal component analysis (PCA). Long-timescale unbiased MD allows us to sample a significant portion of the conformational space available to a given protein, without biasing the population density. The use of GMD analysis allows us to pinpoint significant transitions between conformations or clusters of conformations, without relying solely on clustering or PCA (16).

Previous work done by Abdeen et al. (17) provided a starting point for such work. Here, two of the inhibitory peptides with potentially different modes of action were selected for detailed analysis. These experiments were performed as part of the process of characterizing these peptides. Both peptides inhibit RhoA glucosylation, however, binding affinity did not correlate with inhibitory potential, and only one of the two peptides interfered with glucosylhydrolase activity. This would suggest that even though the end result is the same, the peptides may inhibit TcdB in different ways, possibly through disruption of the intrinsic motions of the protein. By applying MD followed by GMD and PCA, it was determined that a conformational selection mechanism is likely at work in this system. The specific consequences of substrate presence in the active site were determined with respect to the subsets of conformational space contingent on substrate binding.

METHODS

All simulations were carried out using NAMD (18) with the CHARMM27 (19) force field. It is well known that this force field has a tendency to prefer helical structures (20,21). Previous long timescale simulations did not show significant formation of helical structures in crystallographically unstructured regions (14), based on these results we decided to continue our studies with the CHARMM27 force field. The Apo simulation was prepared by removal of the crystallographic UDP and Glucose as previously described. Bound conformations for UPG, HQSPWHH, and EGWHAHT were generated using the LeadIT (22–26) suite for docking. Docking parameters were tested using the crystallographic UDP conformation as proof of method, as published previously (17). All substrates were initially built and minimized at the AM1 level of theory using Spartan 03 (Wavefunction, I. V. K. A., Irvine, CA) and docked into a sphere encompassing all residues within 20 Å of the catalytic manganese. All crystallographic waters were retained and used as both fully rotatable and displaceable. Triangle matching was used for base fragment placement, and dockings were performed with 2000 solutions per each iteration and fragmentation. The standard scoring scale based on Böhm's scoring algorithm (28–30) was employed. Docking was carried out against dynamically relaxed structures following simulation of the apo toxin from a previous work (14) as well as the crystal structure. Following docking to the crystal, 60 and 80 ns structures, clustering was carried out.

Force field parameters for UDP-glucose were created both de novo from single point calculations and by generalization. UDP-Glucose was built in Spartan and initially optimized at the AM1 level of theory. Restricted Hartree-Fock optimization at the 6-31G* level of theory was performed using

Gaussian 03 (26). The optimized geometry was used for frequency calculation, NPA, and ESP charge fitting. Paratool (31) was used to convert the Gaussian output into CHARMM format parameters for comparison with the manually determined parameters. Parameterization by generalization was performed using the parameters from UTP for the UDP after removal of the terminal phosphate. CHARMM parameters for glucose were readily available and parameters for the sugar-UDP linkage were obtained from those determined for phosphoserine. Comparison of parameters derived from these two methods indicated that they were identical within the decimal places used by the standard CHARMM force field.

MD simulations were run on the Wayne State University (WSU) rocks cluster. The canonical ensemble was maintained via periodic boundaries, with Langevin dynamics and thermostat (32). Simulation stability was verified by use of the trajectory analysis tools available with the VMD software (31). Stability was monitored by energy and root mean-square deviation (RMSD). The systems were solvated with TIP3P water, neutralized with counter ions, and subjected to 1000 steps of conjugate gradient minimization and temperature ramped to 300 K. Frames from the trajectories were written every 1 ps. The solvation box includes a 15 Å pad on each face of the box. Long-range electrostatic effects were taken into account using the smooth particle mesh Ewald method (33), and van der Waals interactions were calculated with a nonbonded cutoff of 8 Å and a switching function between 7 and 8 Å. Results were analyzed by use of GMD graphs, via TimeScapes (16), and by PCA using the bio3d package for R. Hydrogen bond and salt-bridge analysis was performed using VMD. All hydrogen bonds and salt bridges occurring for >90% of the simulation time were noted. RMSDs were calculated using VMD.

Clustering was carried out on both MD and docked peptide conformations. Standard clustering in Chimera was performed (34). Cross-comparison of the docked and MD conformations was carried out by superposing all conformers from the docking clusters onto representative structures from the MD clustering. RMSDs between best matching pairs were calculated, and the docking cluster to which they belonged was identified for rank comparison.

RESULTS AND DISCUSSION

Four simulations were carried out to study the inhibitory peptides EGWHAHT and HQSPWHH. For the purpose of the description below, we will refer to EGWHAHT as peptide 1 (P1) and to HQSPWHH as peptide 2 (P2). TcdB was also simulated in the Apo conformation, and bound to its native substrate UDP-Glucose (UPG). Peptide-bound conformations were created by docking using LeadIT, and then performing MD simulations of the docked structures according to the protocol described in the Methods section. All simulations were carried out for 75 ns under unbiased conditions. Analysis was performed using PCA and GMD. All simulations completed normally, and observation of RMSD and total energy indicated that they were continuously stable. The docked structures are shown in Fig. 2, where EGWHAHT is shown in panel *A* in red and HQSPWHH is presented in panel *B* in green. Both peptides bind in the active site, interacting with the yellow mobile loop and purple active site flap. The active site conformation shown in the docking is consistent the mass spectrometric analysis of peptides cross-linked to TcdA (17). Following completion of the dynamics a comparison between docking clusters and dynamics peptide conformations was carried out, to verify agreement between both methods.

A complete clustering analysis workflow is shown in Fig. S1 in the Supporting Material. Following docking to several previously analyzed conformations of TcdB, peptide-bound conformations were simulated. All docking results as well as the two MD simulations were clustered, see Tables S1–S3. To assess the representation of peptide conformations in both the docking and MD simulated structures, a cluster comparison was performed. All docking conformations were superposed on representative structures from the four most populated clusters from the MD. In all cases, following superposition, RMSDs were calculated and cluster membership assessed. As shown in Table S4, the conformations represented in the MD studies are overwhelmingly represented within the top four clusters of the dockings from each state. Backbone RMSDs for all paired structures are <1.1 Å (for a *visual comparison* see Fig. S2). The backbone representation of representative members of the top four clusters from the MD is shown as a block ribbon, whereas the side chains are shown as wire.

Solvent contributions are increasingly regarded as important for protein-small molecule interactions as shown by Kaszuba et al. (35). An analysis of hydrogen bonding and salt bridges was performed to look for solvent interactions and other significant contributions to the stability and coordinated motions of the protein. All interactions present for >90% of the frames were subjected to further analysis and are listed in Table 1. Although the overall number of H-bonds fluctuates from frame to frame, solvation of the active site behaves differently. Hydrogen bonds related to

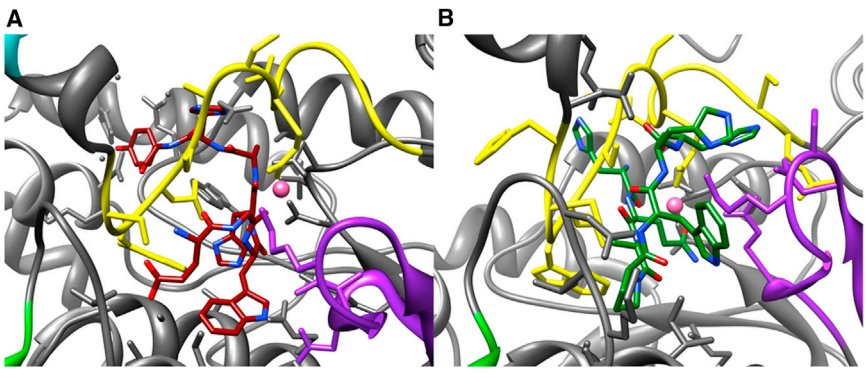

FIGURE 2 Docked conformations of inhibitory peptides. Panel *A* shows EGWHAHT in red, panel *B* shows HQSPWHH in green. Both docked peptides interact with the catalytic mobile loop in yellow, and the active site flap in purple. Catalytic manganese is shown in pink.

TABLE 1 Water hydrogen bonding and salt bridge analysis of MD simulations; Apo-TcdB, UPG, P1, and P2 bound

Interactions	Apo	UPG	P1	P2
Total solvent H-bonds	81	77	87	74
Active site solvent H-bonds	1	0	0	2
Protein binding interface solvent H-bonds	1	1	1	1
Salt bridges	77	58	58	74

Total, active site, protein-interface water hydrogen bonds were measured for all four simulations. We observed between 74 and 81 stable water-protein hydrogen bonds for these simulations. Water-protein interactions were considered stable if they were present for 90% or more of the total frames of the trajectory. An active site water observed in the Apo simulation was not observed in either the UPG- or P1-bound simulations. In the P2-bound simulation, this water is observed with the addition of a second stable water in the active site. All four simulations maintained the same stable protein-interface hydrogen bond. The overall numbers of salt bridges between the Apo and P2 simulations are similar, whereas salt bridging in the P1 simulation better resembles the UPG-bound state.

the regions described previously have been tabulated separately. The active site for the purposes of this analysis was defined in the same way as it was for the docking. The Apo- and P1-bound simulations show higher numbers of H-bonds overall, whereas the UPG- and HQ-bound simulations show fewer interactions. In all simulations, one water molecule remains stationary, interacting with residue E472 on the TcdB-RhoA recognition face. In the UPG- and P1-bound simulations, no stationary waters are observed in the active site. The Apo simulation contains one active site water molecule, and the P2-bound simulation contains two. Hydrogen bonding is observed between solvent water and residue D286 of the DXD motif in both cases. This indicates that P2 is not interacting with the active site in the same way that P1 is, and that P2 preserves the active site hydration observed in the Apo simulation. Salt bridge analysis echoes these results with a higher overall number of salt bridge interactions in the Apo and P2 simulations, and fewer in the UPG and P1 simulations. Again, this reiterates that P1 is mimicking the UPG-bound behavior, whereas P2 is not. Complete lists of all hydrogen bond participants and percentage occupancy in simulation are available in Tables S5–S8. Complete lists of all salt bridge pairs are available in Tables S9–S12.

Principal component analysis was performed to determine the effects of peptide binding on protein structure and flexibility. Following simulation, the principal components of each trajectory were extracted and plotted along with the contribution of each eigenvalue to the total variance as shown in Fig. 3. It is apparent that the binding of the three substrates (UPG, P1, and P2) each has an effect on the conformational space that TcdB explores. In columns 1 and 2, principal component structures are overlaid for each simulation. A widened ribbon in these plots indicates motion, whereas narrow ribbons indicate residues that remain relatively stationary. Column 3 contains the cross-plots of principal components 1 and 2 (PC1 and PC2), in essence, giving a two-dimensional representation of the conformational space that the protein structure is occupying. Because the simulations were projected onto the same core residues for the PC decomposition, all plots in column three are comparable. Column four breaks down the variance in the simulation into contribution by each individual eigenvalue, i.e., the point with the highest proportion of variance is principal component one. The distribution of points along the plotted line indicates the relative contribution to the overall motion from each component eigenvalue. Cross-plots of lower rank principal components for all trajectories are available in Figs. S4–S7.

The Apo simulation shows a high degree of flexibility in both mobile loops, as well as considerable wagging of the four-helix bundle at the N-terminus of the structure. The first principal component, PC1 largely describes this motion, whereas the second captures the side-to-side scissoring of the two promontories shown in cyan (described in Fig. 1). The cross-plot of these two principal components shows an organized set of conformations connected by smooth transitions. The variance contribution of these principal components shows that 36% of the variance in conformation is captured by the wagging motion of the four-helix bundle, and 19% by the scissoring motion. All other motions are captured in lower rank eigenvalues.

The UPG-bound simulation shows less flexibility than the Apo simulation, which is to be expected upon binding of a natural substrate. PC1 is again the wagging of the N-terminal four-helix bundle, whereas PC2 is a distributed motion, not specific to any single region. The cross-plot of principal components shows contraction of the conformational space, particularly with respect to the second principal component. The proportion of variance between the first and second eigenvalues is comparable to the Apo structure.

Peptide 1 binding appears to induce modifications in both the nature of the principal components and the distribution of variance. PC1 again is the wagging of the four-helix bundle, but the motion becomes exaggerated relative to both the Apo- and UPG-bound simulations. PC2 is very similar to that of the UPG-bound simulations, with very little motion in the active site apparent in either principal component. The cross-plot of principal components shows a pattern that appears to be somewhat intermediate between the cross-plots of the Apo- and UPG-bound structures described previously. We interpret this result as an indication that peptide 1 is inhibiting TcdB by mimicking UPG to a great extent. It has previously been shown by Abdeen et al. (17) that peptide 1 is competitive with UPG and can be displaced at high concentrations of UPG. Interestingly, the proportion of variance of the first principal component is considerably higher than for either the UPG or Apo structures, with 52.9% of the variance in the conformational space due to the wagging of the four helix bundle and moderate motion around the active site.

The simulation of peptide 2 bound to TcdB shows considerable alteration in both the principal components and

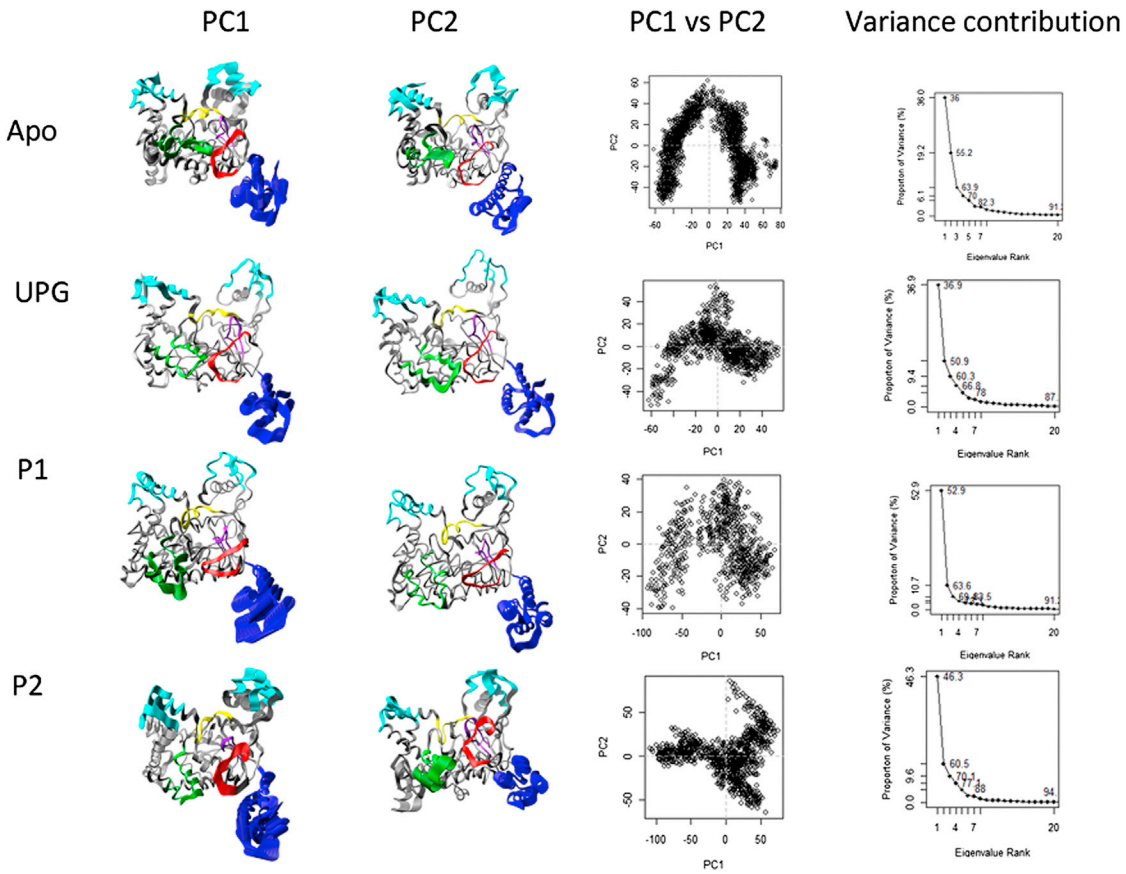

FIGURE 3 PCA analysis of MD simulations; Apo-TcdB, UPG, P1, and P2 bound. Simulations are organized by row, analyses by column. Principal component 1 of each simulation is shown in column 1, principal component 2 is shown in column 2. All structures are colored as in Fig. 1 for comparison. Cross-plots of the first two principal components are shown in column three. PC1 and PC2 are plotted on the *X* and *Y* axes, respectively. Column four presents the contribution of all calculated principal components to the total variance as a percentage. Proportion of variance is plotted against eigenvalue rank to allow assessment of the relative weight of each component.

distribution of variance. PC1 shows motion in the upper promontories, as well as the RhoA recognition site, something unseen in prior simulations. PC2 indicates scissoring of the promontories, albeit in a different direction than observed previously. Additionally, major rearrangements of the RhoA recognition site are observed. The cross-plot of the first and second principal components bears little resemblance to any of the other simulations, and the contributions to the variance are moderately distributed. Abdeen at al. previously showed that peptide 2 is not competitive with UDP-glucose, thus using a distinctly different mechanism for inhibition. This evidence suggests that TcdB uses a conformational selection mechanism (14) and that deformation of the substrate binding site, rather than direct substrate competition is sufficient to achieve inhibition. This may be an effective avenue for inhibitor design because avoiding direct competition with a natural substrate is desirable to achieve maximum efficacy. The sum of these analyses leads us to believe that peptide 2 inhibits TcdB by perturbing the RhoA-binding site, rather than by mimicking UDP-Glucose, whereas peptide 1 represents a relatively classical competitive binding mode of inhibition.

Analysis of the simulations by PCA indicates that the UPG- and peptide-bound conformers have restricted flexibility relative to the apo conformation as expected. However, the inhibitory peptides display differing behaviors with respect to their conformational restriction. As was previously shown by Abdeen et al., (17) peptides show inhibitory potential by either interfering with RhoA or UPG binding. The spatial freedom exhibited by the apo toxin indicates that it is likely that TcdB is subject to a conformational selection and induction mechanism similar to that of the small G-proteins (13). Because TcdB must recognize RhoA and it is undergoing significant motions in response to its own conformational selection process, it makes logical sense that its binding partners, TcdB in this case, might also exhibit similar conformational selection behavior. The dramatic perturbation of the conformational space of TcdB upon contact with the inhibitory peptides, may illustrate a good way to identify proteins involved in conformational selection and study the way they interact with their substrates and/or targets.

To quantitate these results, total as well as local backbone RMSDs of the regions described in Fig. 1 were calculated

and are shown in Table 2. The RMSD overall for the Apo simulation is higher in all regions with the exception of the two protein-protein interface regions, which are dramatically perturbed in the P2-bound simulation. This result is in agreement with the PCA analysis where perturbation of these regions was a major component of the motion. The UPG-bound simulation shows a low RMSD in all regions, again in agreement with the PCA analysis. The P1-bound simulation shows some increased movement in the protein-protein interface regions, whereas both the mobile loop and active site flap behave similarly to the UPG-bound simulation. The combination of the qualitative PCA with the quantitative local RMSD breakdown shows good agreement.

GMD analysis was used to determine the effects of substrate binding on the relative rate of conformational activity. GMD assesses the activity of a simulation, by creating a masked Delaunay representation of the protein structure, and using it to determine how frequently side chains exhibit significant and persistent motion (16). As this is a sliding window analysis, the presented data have been truncated to remove artifacts that occur at the end of these plots. Additionally, we performed these analyses on three nonoverlapping 10 ns segments of each of the trajectories; the plots indicate stability with no major trajectory-wide rearrangements. The plots have been included in Fig. S3 to allow comparison of simulation stability using this analysis, and have not been truncated to illustrate the mathematical artifacts. We examined the activity pattern across all four simulations, to determine what effect each substrate had on the rate and degree of activity of TcdB. Fig. 4 shows the results of GMD analysis on the four simulations. Column 1 shows plots of activity versus scaled frame, all simulations were scaled to 5% of the total frame count for the finished simulation. Columns 2 and 3 show the decomposition of the activity into contact-forming interactions and contact-breaking interactions.

TABLE 2 Overall and local RMSDs of MD simulations; Apo-TcdB, UPG, P1, and P2 bound

RMSD (Å)	Apo	UPG	P1	P2
Overall	2.475	1.294	1.798	2.101
Promontories	2.09	1.746	1.759	1.967
Mobile loop	1.297	1.247	1.21	1.458
Active site flap	2.509	0.964	0.989	1.172
Binding site green	1.237	1.297	2.464	3.42
Binding site red	1.058	1.216	2.217	3.105
Four helix bundle	2.09	1.629	2.464	2.147

RMSD in angstroms was calculated for the overall trajectory, as well as for each region described in Fig. 1. The Apo simulation shows the highest overall RMSD as well as generally higher local RMSDs for all regions with the exception of the two protein-protein interfaces. The green- and red-binding sites are greatly perturbed by the binding of the P2 peptide with their RMSD reaching over 3 Å. The UPG-bound simulations show the lowest overall RMSDs with low activity in the mobile loop and active site flap. P1 shows similar behavior in the active site, although still perturbing the protein-protein binding sites to some extent.

The Apo simulation shows a high level of flexibility throughout, along with a rapid event pattern. The decomposition of activity shows somewhat more contact breaking than forming, as well as a more steady level of contact breaking. The high number of activity spikes may be indicative of continuous conformational transitions, with low points in activity representing conformations amenable to the approach of a binding partner or substrate. Visual inspection of the trajectory shows a repetitive breathing motion that opens the active site somewhat, possibly accounting for the higher level of contact breaking.

The UPG-bound simulation exhibits a dramatically different activity plot. Following an initial rearrangement, activity steadily declines, until reaching a relatively steady state roughly halfway through the trajectory. A few slow moderate rises in activity occur following this point, but the overall rate of activity remains moderate. The plot of contact-forming events shows a steady decrease, suggesting that the bulk of the conformational change involves some degree of unfolding. Analysis of the conformational trajectory agrees with this interpretation. The active site flap moves away from the catalytic center, presenting the region near the manganese ion for catalysis, presumably to allow binding of a glucosylation partner such as RhoA. It has been previously shown that in the absence of UPG, the active site flap folds down, precluding protein-protein binding (14). The level of contact breaking throughout the UPG simulation shows an initial increase, likely associated with the initial rearrangements due to UPG binding.

Analysis of the P1 simulation shows the same initial rearrangements observed in both the UPG and Apo simulations, with an event pattern intermediate to both. A decrease in activity is observed, similar to the bound form with UPG, but remains at a higher level overall, roughly 1.5–1.75 events per frame. The number and frequency of activity spikes are also intermediate to the Apo- and UPG-bound simulations. Interestingly, the shape of the contact-forming and contact-breaking plots is similar to the Apo simulation, but with an increase in the number and frequency of activity spikes, similar to the Apo simulation. This seems to indicate that P1 is in some way acting as a UPG mimic; upon P1 binding, TcdB takes on activity characteristics of the UPG-bound toxin.

The P2 simulation has an activity pattern disparate from all other simulations. The overall level of activity is higher, with smooth transitions between regions of high and low activity. This pattern is not seen in any of the other simulations. The level of contact forming is somewhat lower than the level of contact breaking overall. More rapid transitions in the level of contact making are apparent in the second half of the simulation, whereas no such pattern is observed in the contact breaking activity. The distinct alteration in the event pattern may in some way be contributing to P2's ability to inhibit TcdB. While bound, it appears to disrupt the native pattern of conformational searching, but

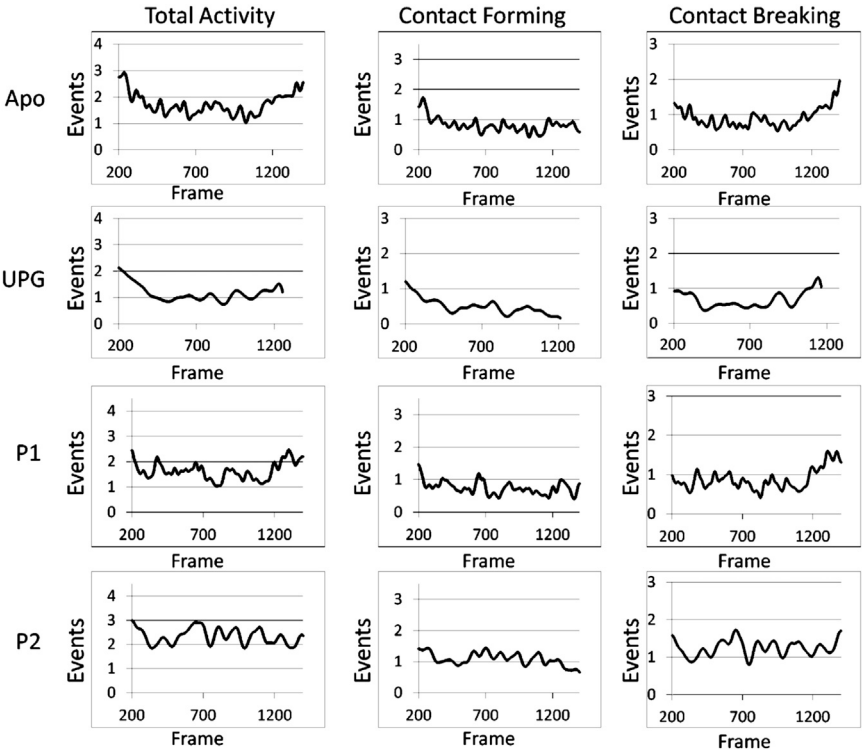

FIGURE 4 GMD analysis of MD simulations; Apo-TcdB, UPG, P1, and P2 bound. As in the PCA analysis, simulations are organized by column, analyses are organized by row. Column 1 shows the total activity of each simulation as a function of frame. The counts of significant persistent events are plotted on the *Y* axis, against simulation progress on the *X* axis. Columns 2 and 3 decompose the total activity into contact-forming events and contact-breaking events.

in an entirely different way than P1. No similarity is evident between the P2-bound and UPG-bound simulations, suggesting that P2 is not acting as a UPG mimic.

In general, this method of determining potential mechanisms of inhibition is rapid, cost-effective, and can be used to distinguish drug candidates with desirable properties for inclusion or exclusion from candidate pools. In any system where a conformational selection mechanism is at work, or even in systems where the protein of interest has multiple targets, the methods described may improve selection of drug leads. Of immediate interest are the other clostridial glucosylating cytotoxins, which may benefit from targeted studies of this nature.

CONCLUSIONS

This work shows that we were able to determine computationally the mode of action of two inhibitory peptides by analyzing the way in which they affect the mobility and conformations of their target. Comparative analysis to Apo and UPG containing simulations allowed for a rapid and effective determination of the effects of peptide binding. The sum of these methods provides excellent context for rational drug lead selection when the method of inhibition is in question.

Previous experiments have shown that the peptides P1 and P2 are capable of inhibiting the glucosyltransferase domain of both TcdA and TcdB. The experimental behavior of P1 and P2 are fundamentally different however, with P1 being a tight binder but poor inhibitor and P2 being a weaker binder but better inhibitor. It was also shown experimentally that P2 is not competitive with UPG, whereas P1 is despite both peptides being identified in the same phage display experiment.

MD simulations and PCA analysis was used to determine the overall effects of substrate binding on TcdB structure and exploration of conformational space. H-bond analysis, salt bridge analysis, and local RMSDs were used to give quantitative context to the differences in the simulations. GMD analysis was used to determine the time-dependent effects of peptide binding on TcdB. By tracking the activity of the simulation through the simulation time, it is possible to observe alterations in the dynamic behavior of a protein that are not linked solely to conformation.

Both GMD and PCA indicated that a major difference between Apo- and UPG-bound TcdB, is the overall motility of the protein. Binding of UPG was shown by PCA to restrict the conformational space of TcdB, and by GMD it was observed to decrease the overall activity of the simulation overall as well. Binding of P1 produces an activity pattern intermediate to the bound and unbound conformations, with dynamic characteristics of each. Our work agrees with the experimental evidence that P1 acts as a UPG mimic. PCA shows that P2 is forcing TcdB into conformations that neither P1 nor UPG are capable of inducing. Dramatic perturbation of the RhoA-binding site is observed, as well as deformation of the upper promontories. Binding of P2 induces a high level of activity along with a distinctly altered event pattern. It is likely that the alteration we observe in the RhoA-binding site and overall activity of

TcdB upon P2 binding is responsible for the inhibitory action of P2. TcdB and other glucosyltransferases are known to use a conformational selection mechanism to find their binding partners, and dramatic disturbance of this process may lead to effective inhibition.

Designing inhibitors to target proteins that use a conformational selection mechanism may prove efficacious. Functionalization of P2 to bind irreversibly gives 95% cell protection during in cellulo assays (S.J. Abdeen, R.J. Swett, S.M. Kern, Y.-W. Nei, M.T. Rodgers, A.L. Feig, unpublished). Increasing numbers of drug targets are being found to employ a conformational selection mechanism. Determining when and if interference in a conformational selection mechanism is occurring may potentially lead to better drug design. To this end, application of MD in conjunction with PCA and GMD analysis may provide insight when developing novel antitoxin agents.

SUPPORTING MATERIAL

Seven figures and twelve tables are available at http://www.biophysj.org/biophysj/supplemental/S0006-3495(13)00614-0.

We thank Sanofar Abdeen and other members of the Feig and Cisneros Laboratories for their helpful discussions on the work.

This work was supported by funds from Wayne State University, Office of the Vice President for Research and the Department of Chemistry. R.J.S gratefully acknowledges support of a Rumble Fellowship from the WSU Graduate School.

REFERENCES

1. Bartlett, J. G., T. W. Chang, …, A. B. Onderdonk. 1978. Antibiotic-associated pseudomembranous colitis due to toxin-producing clostridia. *N. Engl. J. Med.* 298:531–534.
2. Coia, J. E. 2009. What is the role of antimicrobial resistance in the new epidemic of *Clostridium difficile*? *Int. J. Antimicrob. Agents.* 33(*Suppl 1*):S9–S12.
3. Hookman, P., and J. S. Barkin. 2009. *Clostridium difficile* associated infection, diarrhea and colitis. *World J. Gastroenterol.* 15:1554–1580.
4. Huang, H., A. Weintraub, …, C. E. Nord. 2009. Antimicrobial resistance in *Clostridium difficile*. *Int. J. Antimicrob. Agents.* 34:516–522.
5. Gerding, D. N. 2004. Clindamycin, cephalosporins, fluoroquinolones, and *Clostridium difficile*-associated diarrhea: this is an antimicrobial resistance problem. *Clin. Infect. Dis.* 38:646–648.
6. Wüst, J., and U. Hardegger. 1988. Studies on the resistance of *Clostridium difficile* to antimicrobial agents. *Zentralbl. Bakteriol. Mikrobiol. Hyg. [A].* 267:383–394.
7. Jank, T., and K. Aktories. 2008. Structure and mode of action of clostridial glucosylating toxins: the ABCD model. *Trends Microbiol.* 16:222–229.
8. Jank, T., T. Giesemann, and K. Aktories. 2007. *Clostridium difficile* glucosyltransferase toxin B-essential amino acids for substrate binding. *J. Biol. Chem.* 282:35222–35231.
9. Geissler, B., R. Tungekar, and K. J. F. Satchell. 2010. Identification of a conserved membrane localization domain within numerous large bacterial protein toxins. *Proc. Natl. Acad. Sci. USA.* 107:5581–5586.
10. Reinert, D. J., T. Jank, …, G. E. Schulz. 2005. Structural basis for the function of *Clostridium difficile* toxin B. *J. Mol. Biol.* 351:973–981.
11. Egerer, M., T. Giesemann, and K. Aktories. 2007. Auto-catalytic cleavage of Clostridium difficile toxins A and B depends on a cysteine protease activity. *J. Biol. Chem.* 282:25314–25321.
12. Giesemann, T., M. Egerer, …, K. Aktories. 2008. Processing of *Clostridium difficile* toxins. *J. Med. Microbiol.* 57:690–696.
13. Grant, B. J., J. A. McCammon, and A. A. Gorfe. 2010. Conformational selection in G-proteins: lessons from Ras and Rho. *Biophys. J.* 99:L87–L89.
14. Swett, R., G. A. Cisneros, and A. L. Feig. 2012. Conformational analysis of *Clostridium difficile* toxin B and its implications for substrate recognition. *PLoS ONE.* 7:e41518.
15. Boehr, D. D., R. Nussinov, and P. E. Wright. 2009. The role of dynamic conformational ensembles in biomolecular recognition. *Nat. Chem. Biol.* 5:789–796.
16. Wriggers, W., K. A. Stafford, …, D. E. Shaw. 2009. Automated event detection and activity monitoring in long time-scale molecular dynamics. *J. Chem. Theory Comput.* 5:2595–2605.
17. Abdeen, S. J., R. J. Swett, and A. L. Feig. 2010. Peptide inhibitors targeting *Clostridium difficile* toxins A and B. *ACS Chem. Biol.* 5:1097–1103.
18. Phillips, J. C., R. Braun, …, K. Schulten. 2005. Scalable molecular dynamics with NAMD. *J. Comput. Chem.* 26:1781–1802.
19. Brooks, B. R., C. L. Brooks, 3rd, …, M. Karplus. 2009. CHARMM: the biomolecular simulation program. *J. Comput. Chem.* 30:1545–1614.
20. Best, R. B., N. V. Buchete, and G. Hummer. 2008. Are current molecular dynamics force fields too helical? *Biophys. J.* 95:L07–L09.
21. Cino, E. A., W. Y. Choy, and M. Karttunen. 2012. Comparison of secondary structure formation using 10 different force fields in microsecond molecular dynamics simulations. *J. Chem. Theory Comput.* 8:2725–2740.
22. Rarey, M., B. Kramer, …, G. Klebe. 1996. A fast flexible docking method using an incremental construction algorithm. *J. Mol. Biol.* 261:470–489.
23. Miteva, M. A., W. H. Lee, …, B. O. Villoutreix. 2005. Fast structure-based virtual ligand screening combining FRED, DOCK, and Surflex. *J. Med. Chem.* 48:6012–6022.
24. Degen, J., and M. Rarey. 2006. FlexNovo: structure-based searching in large fragment spaces. *ChemMedChem.* 1:854–868.
25. Schellhammer, I., and M. Rarey. 2004. FlexX-Scan: fast, structure-based virtual screening. *Proteins.* 57:504–517.
26. Frisch, M. J., H. B. Schlegel, …, J. A. Pople. 2004. Gaussian 03.
27. Reference deleted in proof.
28. Huang, S. Y., and X. Q. Zou. 2010. Inclusion of solvation and entropy in the knowledge-based scoring function for protein-ligand interactions. *J. Chem. Inf. Model.* 50:262–273.
29. Huang, S. Y., and X. Q. Zou. 2006. An iterative knowledge-based scoring function to predict protein-ligand interactions: I. Derivation of interaction potentials. *J. Comput. Chem.* 27:1866–1875.
30. Gohlke, H., M. Hendlich, and G. Klebe. 2000. Knowledge-based scoring function to predict protein-ligand interactions. *J. Mol. Biol.* 295:337–356.
31. Humphrey, W., A. Dalke, and K. Schulten. 1996. VMD: visual molecular dynamics. *J. Mol. Graph.* 14:33–38, 27–28.
32. Izaguirre, J. A., D. P. Catarello, …, R. D. Skeel. 2001. Langevin stabilization of molecular dynamics. *J. Chem. Phys.* 114:2090–2098.
33. Wang, H., F. Dommert, and C. Holm. 2010. Optimizing working parameters of the smooth particle mesh Ewald algorithm in terms of accuracy and efficiency. *J. Chem. Phys.* 133:034117.
34. Kelley, L. A., S. P. Gardner, and M. J. Sutcliffe. 1996. An automated approach for clustering an ensemble of NMR-derived protein structures into conformationally related subfamilies. *Protein Eng.* 9:1063–1065.
35. Kaszuba, K., T. Róg, …, M. Karttunen. 2010. Molecular dynamics simulations reveal fundamental role of water as factor determining affinity of binding of beta-blocker nebivolol to beta(2)-adrenergic receptor. *J. Phys. Chem. B.* 114:8374–8386.